Dynamic simulation of crack initiation and propagation in cross-ply laminates by DEM

Dongmin Yang, Yong Sheng, Jianqiao Ye, Yuanqiang Tan

Dynamic simulation of crack initiation and propagation in cross-ply laminates by DEM

Dongmin Yang, Yong Sheng, Jianqiao Ye, Yuanqiang Tan

PII: S0266-3538(11)00188-6
DOI: 10.1016/j.compscitech.2011.05.014
Reference: CSTE 4994

To appear in: *Composites Science and Technology*

Received Date: 1 March 2011
Revised Date: 9 May 2011
Accepted Date: 22 May 2011

Please cite this article as: Yang, D., Sheng, Y., Ye, J., Tan, Y., Dynamic simulation of crack initiation and propagation in cross-ply laminates by DEM, *Composites Science and Technology* (2011), doi: 10.1016/j.compscitech.2011.05.014

Dynamic simulation of crack initiation and propagation in cross-ply laminates by DEM

Dongmin Yang[1, 2], Yong Sheng[1], Jianqiao Ye[1,*], Yuanqiang Tan[2]
1. School of civil engineering, University of Leeds, Leeds LS2 9JT, UK
2. School of mechanical engineering, Xiangtan University, Hunan 411105, China

Abstract

A representative element of the cross-ply laminate was modeled by the discrete element method (DEM) to analyze the stresses distribution. The DEM modeling results were compared with those from alternative approaches to validate the DEM model. The transverse cracking and interfacial delamination in $[0^\circ_1/90^\circ_3]_s$ and $[90^\circ_n/0^\circ_1]_s$ cross-ply laminates under transverse loading were analyzed by comparing crack densities as well as stiffness reduction with those from experiments and other numerical methods. It was found that the proposed DEM model can simultaneously capture the transverse cracking and delamination phenomenon, and can predict the variation of crack density and stiffness reduction accurately.

Keywords: cross-ply laminates; stress distribution; transverse cracking; delamination; stiffness reduction; DEM

1. Introduction

Fiber reinforced composites have many attractive material properties characterized by the high strength and stiffness to mass ratios, damage tolerance and corrosion resistance, making them suitable for many structural applications such as wind turbine, armor, naval and aerospace structures [1]. A major concern in the use of composite materials is the susceptibility to damage resulting from the intrinsic microstructures under complicated external loading. Due to the complex nature of fiber reinforced composite materials, the onset of damage does not cause instantaneous failure of the entire structure. More often transverse cracking and delamination are typical damages taking place before the final catastrophic failure when the cross-ply laminates are subject to transverse tensile loading [2]. Transverse cracking can be initiated from the defects of matrix or after the fiber/matrix interfacial debonding caused by the tensile stress in the 90^o ply. Delamination is normally initiated by the shear stress concentrating between the two neighboring plies due to the dissimilar material properties of the two adjacent plies, under the action of transverse loadings or free-edge stresses.

Therefore, the analysis of stress distribution is of critical importance for the prediction of damage and the application of appropriate failure criteria. Theoretical solutions of stress distribution have been achieved by using different analytical models, such as the

* Corresponding author. Email: j.ye@leeds.ac.uk

classical laminate theory (CLT) [3, 4], the full layer-wise theory [5] and the stress transfer model [6, 7]. Finite element method (FEM), as one of the most commonly used numerical methods for stress analysis, has also been used to compute the interlaminar stress distribution [8]. However, FEM is sometimes time consuming and even unreliable when high order singularities occur [9]. Ye et al. [10] developed a state space finite element method, which is a semi-analytical method, to solve the stress singularities in the vicinity of free-edge or localized traction free surface by combining the traditional finite element approximation and the recursive formulation of state space equation.

Even though many methods can properly predict the stress distribution in composite laminates under various loading conditions, few of them can be applied to describe the progressive damage behaviors, e.g., the initiation and propagation of transverse cracking and/or delamination. The onset of transverse cracking is normally predicted by a damage analysis model using either a strength based theory [11] or the critical fracture energy release rate [12] as failure criterion.

The study of delamination has attracted continuous attention of the composite researchers. Fracture mechanics, such as linear elastic fracture mechanics (LEFM), was employed in the study of propagation of a pre-defined or existing crack. However, it cannot characterize crack initiation [13]. Interface element was also proposed in FEM analysis to represent the interface where delamination may occur. Chen et al. [14] implemented interface elements, which were characterized by a linear decohesion model, into FEM software packages to predict progressive delamination of composite materials. Bruno et al. [15] analyzed the mix mode delamination by coupling the interface elements approach and fracture mechanics with the consideration of crack-faces interaction. Wagner et al. [16] argued that mesh refinement in FEM may not necessarily lead to a converged solution and presented a softening interface element with non-vanishing thickness to simulate growing delamination in composite structures. Nishikawa et al. [17] developed an updating-element technique, in which near the damage process zone a fine mesh was located and varied automatically, to reduce the computational cost of simulating delamination in CFRP cross-ply composite under transverse loading. To overcome crack closure problems, cohesive zone model (CZM) has often been implemented into FEM codes to connect two different substructures. The CZM is usually characterized by a bilinear relationship of displacement and traction force, with an imposed maximum strength and maximum amount of facture energy. Hu et al. [18] used a CZM adapted with the explicit central difference algorithm to present the interface damage between matrix and fiber under quasi-static transverse loading. Meo and Thieulot [19] compared CZM with the fracture mechanics models for mode I delamination and observed good correlations. Borg et al. [20] used a discretized cohesive zone model to simulate modes I, II and III crack initiation and propagation. Pantano and Averill [21] proposed a mesh-independent interface method to simulate the mixed-mode delamination growth. Xie and Waas [22] developed a similar CZM model based on discrete spring method, which is found to be independent of mesh size and more computationally efficient. Several other numerical methods were also

proposed to predict the onset and evolution of interlaminar failure and the final collapse, such as continuum damage model (CDM) [23, 24] and boundary element method (BEM) [25].

The interactions of transverse cracking and delamination have also been taken into account by the numerical models developed for the simulation of progressive damage process in cross-ply laminates. Berthelot and Corre [26] presented a statistical model, by which the initiation of transverse cracking and delamination was evaluated according to the local stress values. Okabe et al. [27] used an embedded process zone (EPZ) model in FEM to simulate transverse cracking and interlaminar delamination by assuming that the damage only propagated along the pre-defined embedded process zone. The above mentioned methods have made respective contribution to the study of damage and failure of composite laminates. However, most of them were based on continuum mechanics and could not account for the complex nature of the microstructures of the composite materials. Also, they all faced the difficulties in dealing with the problems such as crack tip singularities and incorporation of dynamic material behaviors. This is the bottleneck that limits the applications of the existing models. On the other hand, the transverse cracking as well as delamination are commonly formed by smaller damage events, such as matrix cracking and fiber/matrix debonding, which take place randomly across the whole material domain. Therefore, the evaluation of transverse cracking and delamination is more realistic and accurate if they are statistically characterized by smaller collective damage events occurring at smaller scale.

As a natural progress of the research in the area of modeling damage at microscopic scales, a discrete element method (DEM) is proposed in this paper to simulate dynamic initiation and propagation of transverse cracking and interlaminar delamination which are characterized by two contact constitutive models, respectively. DEM has been used in our previous research of microbond test [28] and transverse cracking [29] of composite materials. The purpose of this research is not only to validate the application of DEM in terms of its advantages in the simulation of cracking density and stiffness reduction prediction, but also to highlight the potential of DEM in the future research application for composite damage mechanism, composite material design and optimization.

2. Discrete Element Method (DEM)

Discrete element method (DEM) was proposed by Cundall to study the discontinuous mechanical behavior of rock [30] and has been implemented in many other fields, such as geomaterials [31], granular materials [32], concrete [33], ceramics [34]. The particle discrete element method assumes that the particle elements are usually disc in 2D or spherical in 3D due to the simplicity of contact algorithm and the saving of computational time. The contact forces between any two particles are determined from the overlap and relative movements of the particle pair according to a specified force-displacement law. In 2D DEM, the motion of the particles over a time step Δt is governed by Newton's second law as below [30, 32]:

Translational motion $F_i = m(\dot{v}_i - g_i)$ (1)

Rotational motion $M_3 = I\dot{\omega}_3$ (2)

where (i = 1, 2) denotes, respectively, the x-and y- co-ordinate directions, F_i is the resultant force of the particle; v_i is the translational velocity; m is the mass of the particle; g_i is the body force acceleration vector (e.g., the gravity loading); M_3 is the out of balance moment referred to the out-of-plane axis, ω_3 is the rotational velocity about the out-of-plane axis; I is the rotational inertia of the particle; and t is time. Damping, e.g., local damping or viscous damping, can be added into the DEM model to dissipate the kinetic energy together with particles' frictional sliding so as to obtain a steady-state solution more efficiently [35]. Equations (1) and (2) are usually solved by a finite difference scheme. Both the specified force-displacement law and Newton's second motion law are used in the calculation cycle of the discrete element method.

DEM allows particles to be bonded together at contacts and to be separated when the bond strength or energy is exceeded. Therefore it can simulate the motion of individual particles and also the behavior of bulk material which is formed by assembling many particles through bonds at contacts with specific constitutive laws. In a DEM model of bulk material, elementary micro scale particles are assembled to form the bulk material with macroscopic continuum behavior determined only by the interaction of particles [35, 36]. Unlike the traditional solution using the strain and stress relations, contact properties are the predominant parameters in a DEM solution, combined with size and shape of the particles. Subject to external loading, when the strength or the fracture energy of a bond between particles is exceeded, flow and disaggregation of the particle assembly occur and the bond starts to break. Consequently, cracks form naturally at micro scale. Hence, damage modes and their interaction emanate as the process of debonding of particles. The way that DEM discretizes the material domain gives the most significant advantage over the traditional continuum mechanics based methodologies, as the difficulties encountered by the traditional methods, such as dynamic material behavior of composites, crack tip singularities and crack formulation criteria can all be avoided due to the naturally discontinuous representation for the microstructure of composite materials via particle assemblies in DEM.

Wittel et al. [37] constructed a two dimensional triangular lattice of springs to model the $[0/90]_s$ cross-ply laminates based on DEM. The nodes in the lattice model represent fibers, and the springs with random breaking thresholds according to Weibull distribution represent the disordered matrix. Molecular dynamic simulation was used to follow the time evolution. However, the topological disorder of the material was neglected, and the orthotropic behavior of 0° ply and the adhesion of ply-ply interface were not considered in this model.

3. DEM Model of Cross-ply Laminates

3.1 DEM Model of laminae ply

In this paper, 2D DEM model was constructed by using a six-spring hexagonal arrangement as the basic unit, as shown in Fig.1, to represent the composite laminae.

Each contact between the particles is described by a normal spring and a tangential spring with spring constants k_n and k_s, respectively. Therefore, the elastic properties (i.e., elastic modulus and Possion's ratio) of the material are related to the constants of the springs. Sawamoto et al [38], Kim et al. [39], and Taverez and Plesha [40] derived the equations of spring constants for isotropic materials. Liu and Liu [41] proposed a general formula for both anisotropic and isotropic materials, as follows:

$$\begin{cases} \mathrm{k_{n1}} = \frac{\sqrt{3}}{6}(3\mathrm{c_{11}} + 2\mathrm{c_{12}} - \mathrm{c_{22}})\delta \\ \mathrm{k_{n2}} = \frac{\sqrt{3}}{3}(\mathrm{c_{11}} + \mathrm{c_{22}} + \sqrt{3}\mathrm{c_{16}} + \sqrt{3}\mathrm{c_{26}})\delta \\ \mathrm{k_{n3}} = \frac{\sqrt{3}}{3}(\mathrm{c_{11}} + \mathrm{c_{22}} - \sqrt{3}\mathrm{c_{16}} - \sqrt{3}\mathrm{c_{26}})\delta \\ \mathrm{k_{s1}} = \frac{2\sqrt{3}}{3}(3\mathrm{c_{66}} - \mathrm{c_{22}})\delta \\ \mathrm{k_{s2}} = \frac{\sqrt{3}}{3}(\mathrm{c_{22}} - 3\mathrm{c_{12}} + 3\sqrt{3}\mathrm{c_{16}} - \sqrt{3}\mathrm{c_{26}})\delta \\ \mathrm{k_{s3}} = \frac{\sqrt{3}}{3}(\mathrm{c_{22}} - 3\mathrm{c_{12}} - 3\sqrt{3}\mathrm{c_{16}} + \sqrt{3}\mathrm{c_{26}})\delta \end{cases} \quad (3)$$

Where, k_{n1} and k_{s1} are the spring constants at the contacts between particles 0 and 6, and particles 0 and 3; k_{n2} and k_{s2} are the spring constants at the contacts between particles 0 and 1, and particles 0 and 4; k_{n3} and k_{s3} are the spring constants at the contacts between particles 0 and 2, and particles 0 and 5; and δ is the element thickness. c_{ij} (i=6, j=6) are the elastic coefficients of the material stiffness matrix,

$$C = \begin{pmatrix} c_{11} & \cdots & c_{16} \\ \vdots & \ddots & \vdots \\ sym & \cdots & c_{66} \end{pmatrix} \quad (4)$$

For a 2D orthotropic laminae materials (e.g., 0˚ ply), c_{16}=c_{26}=0, and Eq. (3) is reduced to

$$\begin{cases} \mathrm{k_{n1}} = \frac{\sqrt{3}}{6}(3\mathrm{c_{11}} + 2\mathrm{c_{12}} - \mathrm{c_{22}})\delta \\ \mathrm{k_{n2}} = \mathrm{k_{n3}} = \frac{\sqrt{3}}{3}(\mathrm{c_{11}} + \mathrm{c_{22}})\delta \\ \mathrm{k_{s1}} = \frac{2\sqrt{3}}{3}(3\mathrm{c_{66}} - \mathrm{c_{22}})\delta \\ \mathrm{k_{s2}} = \mathrm{k_{s3}} = \frac{\sqrt{3}}{3}(\mathrm{c_{22}} - 3\mathrm{c_{12}})\delta \end{cases} \quad (5)$$

The material stiffness coefficients for an orthotropic material under plane stress condition are calculated as

$$\begin{cases} \mathrm{c_{11}} = \frac{\mathrm{E_1}}{1-\upsilon_{12}\upsilon_{21}} \\ \mathrm{c_{12}} = \frac{\upsilon_{12}\mathrm{E_1}}{1-\upsilon_{12}\upsilon_{21}} \\ \mathrm{c_{22}} = \frac{\mathrm{E_2}}{1-\upsilon_{12}\upsilon_{21}} \\ \mathrm{c_{66}} = \mathrm{G_{12}} \end{cases} \quad (6)$$

For a 2D isotropic material (e.g., 90˚ ply), Eqs.5 and 6 can be simplified as

$$\begin{cases} k_n = \frac{E\delta}{\sqrt{3}(1-\upsilon)} \\ k_s = \frac{E\delta(1-3\upsilon)}{\sqrt{3}(1-\upsilon^2)} \end{cases} \quad (7)$$

As illustrated by Eq.7, the Poisson's ratio of a 2D isotropic material must be smaller than 0.33 for a positive k_s when the hexagonal packing scheme is used.

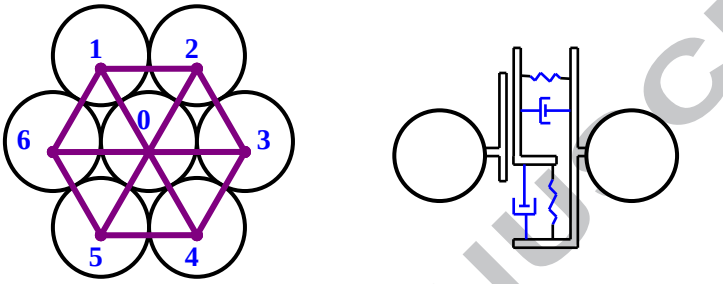

(a) Hexagonal packing (b) Contact between particles

Fig.1 Hexagonal packing of discrete particles

Solid materials are usually modeled by DEM through adding a bond at the contact of two contacting particles. Bonds in DEM can be envisioned as a kind of glue joining the two contacting particles. There are two intrinsic bonds, contact bond and parallel bond in PFC2D [42] that is a popular commercial code of DEM and is used as the simulation platform of this research. A parallel bond can be regarded as a set of elastic springs with constant normal and shear stiffness, uniformly distributed over either a circular or rectangular cross-section lying on the contact plane and centered at the contact point, as shown in Fig.2 [35]. Parallel bond can transmit both forces and moments, and will be used in this paper.

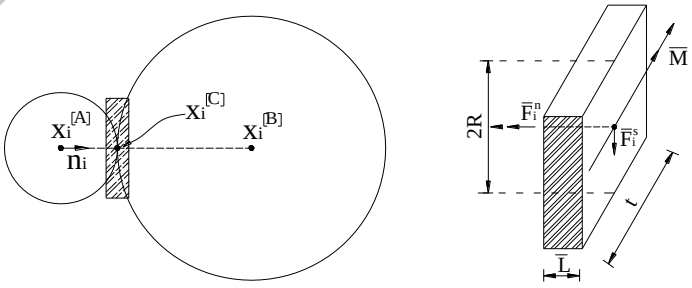

Fig.2 Parallel bond in two dimensional DEM

In the DEM model with parallel bonds, the contact stiffness, K_i, at each particle-particle contact is resulted from both particles' stiffness and parallel bond's stiffness through the following formulations [35],

$$K_i = A\bar{k}_i + k_i \quad (8)$$

$$A = 2\bar{R}\delta \quad (9)$$

$$k_i = \frac{k_i^{[A]} k_i^{[B]}}{k_i^{[A]} + k_i^{[B]}} \quad (10)$$

Where $\bar{R}$ and A are the radius and cross-section area of the parallel bond, respectively. δ is the element thickness, $\bar{k}_i$ is the parallel bond stiffness and k_i is the equivalent stiffness of the two contacting particles. i is in place of n or s which denotes normal or shear direction, respectively. If the two particles in contact have the same normal and shear stiffness,

$$k_i = \frac{k_i^{[A]}}{2} = \frac{k_i^{[B]}}{2} \quad (11)$$

In order to simulate the stiffness of particle assembly dominantly by the parallel bond, the particles' stiffness is set to be much smaller than that of the parallel bond, e.g.,

$$k_i = 0.01 A \bar{k}_i \quad (12)$$

and

$$K_i \approx A \bar{k}_i \quad (13)$$

Therefore the parallel bond stiffness can be calculated by combining Eq.5 and Eq.13, or Eq.7 and Eq.13. The parallel bond has a linear elastic behavior, as shown in Fig.3. The bond breaks when the contact force exceeds its strength [28, 34].

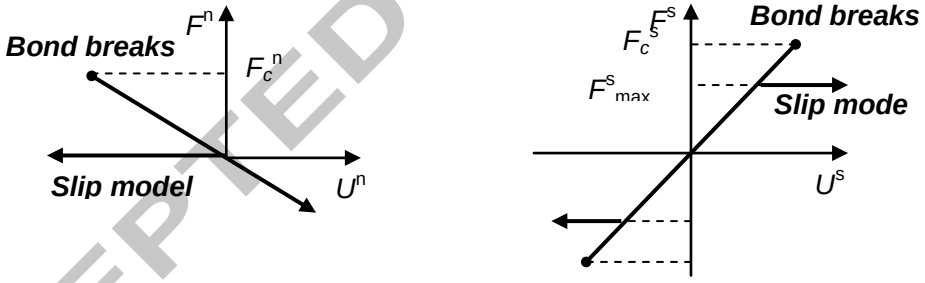

(a) *normal behavior* (b) *shear behavior*

Fig.3 Constitutive behavior of the parallel bond at contact

3.2 DEM Model of Ply-ply Interface

As suggested in [43, 44] that the interface between two composite plies is adhesive, there exist residual interfacial traction forces, even when the two plies are detached but before they are entirely separated. Therefore alternative contact models have been proposed by DEM users to account for the complex interfacial behaviour by considering more complicated constitutive laws. The contact softening model was proposed for this purpose based on the contact bond model [35, 39]. The concept of contact softening model (illustrated in Fig.4) is similar to the cohesive zone model (CZM) in the continuum mechanics [17, 22]. The only difference between these two models is the unloading and reloading curves after yielding.

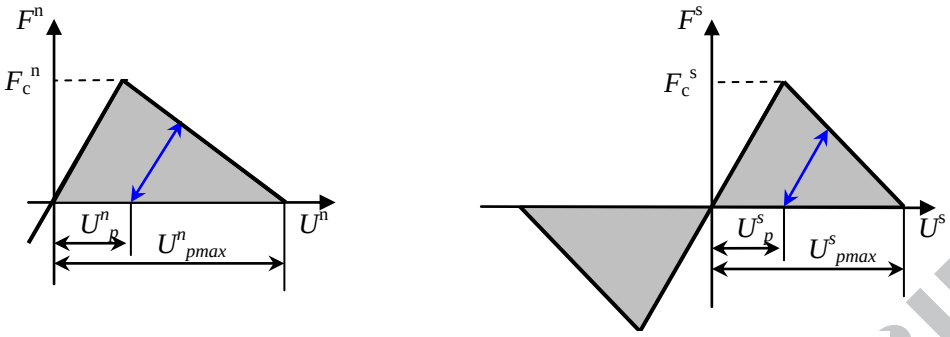

(a) normal behavior (b) shear behavior

Fig.4 Constitutive behavior of contact softening model

The contact softening model describes the behavior of contact bonds in elastic, and represents plastic deformation by linearly softening the bond after the contact force reaches the bond strength. In both tensile and shear situations, the bond strength decreased to zero when the plastic displacement reaches the maximum plastic displacement U_{pmax} which is related to the fracture energy release rate G. The interfacial crack may behavior as mode I, mode II or mix mode according to the stress field at the crack tip. In order to simulate the three fracture modes in DEM, the maximum plastic displacement U_{pmax} was kept constant, while the bond normal and shear strengths were defined individually. Hence, in a two dimensional system, the fracture energy release rate for mode I and mode II are, respectively:

$$G_I = \frac{1}{2} \cdot \sigma_{nmax} \cdot U_{pmax} \tag{14}$$

And

$$G_{II} = \frac{1}{2} \cdot \sigma_{smax} \cdot U_{pmax} \tag{15}$$

In 2D DEM, the contact stresses at the bond are taken as the average stress between the two contacting particles [35], as calculated below:

$$\sigma_{imax} = \frac{F_c^i}{A} = \frac{F_c^i}{2\check{R}\delta} \tag{16}$$

$$\check{R} = \frac{1}{2}(R_1 + R_2) \tag{17}$$

The fracture energy release rate can be calculated as:

$$G = \frac{1}{2} \cdot \sigma_n \cdot U_p^n + \frac{1}{2} \cdot \sigma_s \cdot U_p^s = \frac{1}{2} \cdot \sigma_n \cdot \sum \left|\Delta U_p^n\right| + \frac{1}{2} \cdot \sigma_s \cdot \sum \left|\Delta U_p^s\right| \tag{18}$$

σ_n and σ_s are the normal and shear stresses of the bond when yield occurs. For the mixed mode, the fracture energy release rate is somewhere between the rates of two single fracture modes.

The interface of the laminate is treated as the contact between two single layers of particles that are symmetrically arranged in the DEM model, as illustrated in Fig.5. A detailed study of the progressive interfacial delamination under mode I, mode II as well

as mix mode in composite laminates by DEM is referred to [45], where the specifications for the respective dedicated interfacial delamination models can also be found.

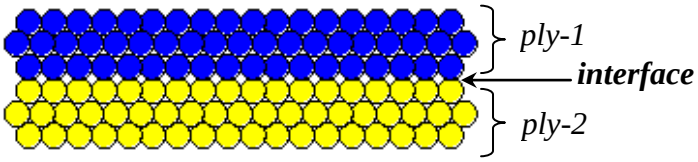

Fig.5 Configuration of interface in DEM model

4. Stress Distribution at Free-edge and Interface

The interlaminar stress distribution close to ply cracks as well as free edge of a laminate was usually studied by a representative element as shown in Fig.6 [6, 10], where it is assumed that the ply cracks (indicated by red lines) are uniformly distributed along the length parallel with the loading direction. This representative element is also adopted in this paper to validate the DEM model by comparising with the solutions from existing studies [46]. In this paper, it is assumed that both the 90º and 0º plies are made of transversely isotropic materials. When the 3D material is reduced to a 2D model, the 90º and 0º plies are equivalently represented by the respective isotropic and orthotropic materials. The stress distribution analysis of a $[0^\circ/90^\circ]_s$ laminate, with the following 2D mechanical properties, was carried out by the developed DEM model.

For the 90º ply: E=14.48 GPa; υ=0.21
For the 0º ply: E_L=137.9 GPa; E_T=14.48 GPa; υ_{LT}=0.21; G_{LT}=5.86 GPa

The geometry of the representative element is assumed to have the width L, and thickness h, with $L = 4h$. Also each of the material layers is of equal thickness $h/4$ and idealized as a homogeneous material. Constant displacement loading was applied on the 0˚ ply at both ends of the element with a constant horizontal velocity of 0.05 m/s , which represents for a quasi-static loading condition [28]. Figure 7 shows the comparisons for the through thickness distribution of the normal stress σ_{xx}. The peeling and shear stresses at the interface of the laminate are plotted and compared, respectively in Fig.8 and Fig.9. It can be observed that the developed DEM model can predict the stress distribution accurately, with the results agreeing very well with those obtained from the space state finite element method [46].

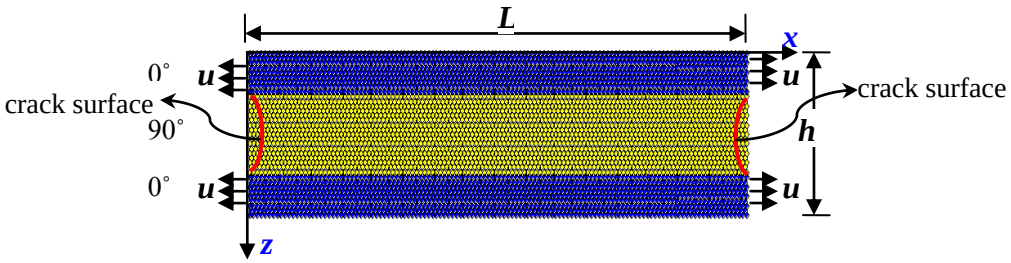

Fig.6 A representative element for cross-ply laminate

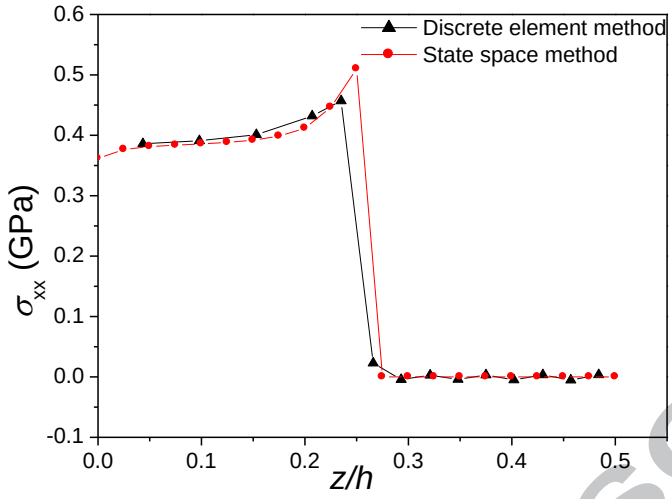

Fig.7 Distribution of axial stress through the thickness at x=0

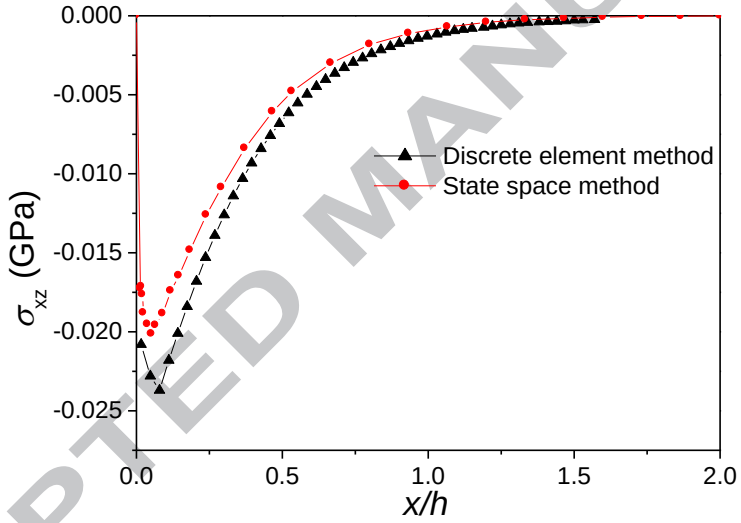

Fig.8 Distribution of interlaminar shear stress at 0˚/90˚ interface

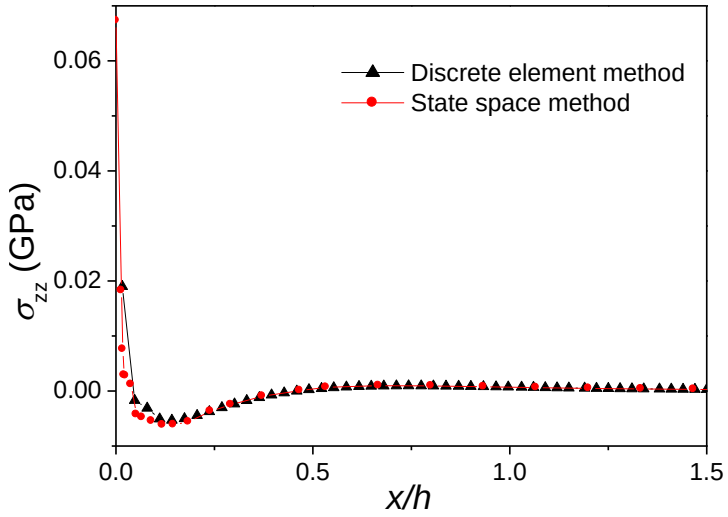

Fig.9 Distribution of interlaminar normal stress at 0˚/90˚ interface

5. DEM Simulation of Transverse and Delamination

The damage in cross-ply composite laminates, e.g., transverse cracking and delamination, can be represented by the breakage of bonds at the contacts of particles in DEM. An example of $[0^{\circ}/90^{\circ}_3]_s$ glass fiber reinforced epoxy laminate is considered in this paper. The results are compared with the statistical analysis in [26] and the experimental studies in [47]. It is worth to mention here that physical delamination of the laminate could be in the form of interfacial delamination, occurring right along the 0^o and 90^o interface, or in the form of cracks in the 90^o plies which are close and parallel to the interface. Therefore, in the examples shown in the remainder of this paper, the terminology 'without interfacial delamination' does not necessarily suggest that there is no physical delamination. The material properties used for the model are as follows:

For the 90^o ply: E=13.0 GPa; υ=0.3
For the 0^o ply: E_L=41.7 GPa; E_T=13.0 GPa; υ_{LT}=0.3; G_{LT}=3.4 GPa

Each ply has a thickness of 0.203 mm and a length of 50 mm, as shown in Fig.10, where the particles with blue and gray colors indicate 0° and 90° plies, respectively. A constant loading velocity was applied at both sides of the specimen, and the average applied loading stress σ_c was recorded. The bond strength in the 0° plies was set to be large enough to avoid any breakage. The tensile strength of the parallel bonds in the 90° plies, $\sigma_{t,}$ was 67 MPa with a variation of 30% following a normal distribution law [26], and the shear strength was assumed much higher to ensure that only tensile failure occurred. Interfacial delamination was not considered initially by applying a sufficiently high interfacial strength. From the DEM dynamic simulation of the damage process, it can be seen that transverse cracking occurs as failure of particle bonds that are relatively weaker, and propagates through the bond breakages, as demonstrated in Fig.10 (a) – (c). The saturated transverse cracks are almost uniformly distributed, and severe damage caused by stress concentration at the tips of the transverse cracks is evident from the DEM results. Interfacial delamination was introduced by setting the interfacial shear strength τ to 48 MPa and the interface fracture energies G_I and G_{II} to 257 J/mm^2 and 856 J/m^2, respectively [14]. A variation of 30% was also introduced to reflect the non uniform distribution of these properties. When interfacial delamination is included, as shown in Fig.10 (d), it occurs at the tips of the transverse cracks, but this does not affect change the distribution of transverse cracks significantly when comparing to Fig.10 (c). However, magnified views of the models with/without interfacial delamination showed that less damage was observed in 90° ply along the interface when interfacial delamination was considered as indicated in Fig.11 (a) and (b). In this study the interface was regarded as delaminated when the interfacial strength was reached (represented by a black line in Fig.10 as well as in Fig.11 with magnified views), even though the fracture energy was not exceeded. The saturation pattern of transverse cracking in the DEM model was found to have a good agreement with the observed experimental results from [47] (see Fig.12).

Quantitative analyses were carried out by counting the number of transverse cracks at selected loading increment in the DEM simulation and plotting the transverse crack density against the average loading stress, as shown in Fig.13. Good agreement of the transverse crack density was found between the DEM simulation and available experimental results [47] and statistical analysis [26]. There is a significant discrepancy when the DEM modeling (without interfacial delamination) was compared with the results from the statistical analysis (without delamination). This was because this dedicated statistical model deals with only transverse cracks while the DEM model allows both transverse cracking and delamination within the 90^o plies. The crack density tends to become saturated in the DEM modeling without interfacial delamination, since the cracks can propagate within the 90˚ ply along the interface through matrix failure (as shown in Fig.11 (a)). The crack density in the statistical analysis model without delamination remains increasing due to the assumption that all cracks occur only in the through-thickness direction. The comparisons show that the crack density in the DEM model without interfacial delamination is greater than the one with interfacial delamination when the loading stress reached about 80 MPa, at which interfacial delamination starts. Since the variation of the 90 plies strength (i.e., 30%) was chosen, it appears that the DEM model with interfacial delamination underestimates the crack density. It suggests that a smaller interfacial strength variation could lead to a better agreement. It is expected that thermal residual stress along the interface might also affect the crack density evolution, which has not been included in the current DEM models.

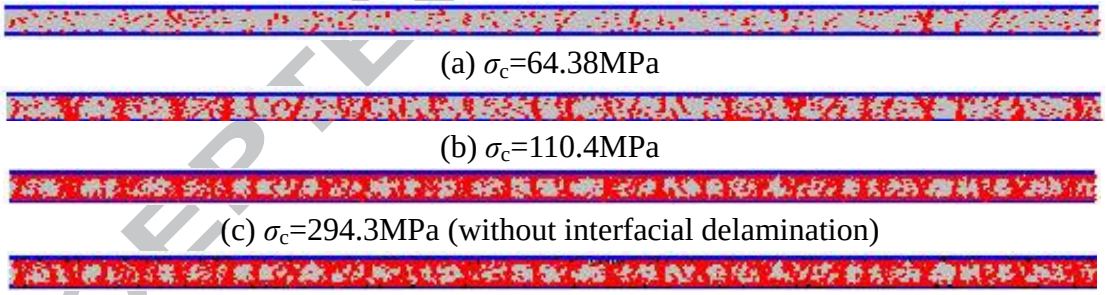

(a) σ_c=64.38MPa

(b) σ_c=110.4MPa

(c) σ_c=294.3MPa (without interfacial delamination)

(d) σ_c=294.3MPa (with interfacial delamination)

Fig.10 Dynamic initiation and propagation of transverse cracking and/or delamination in $[0^\circ_1/90^\circ_3]_s$ cross-ply laminate.

(Particles with blue and gray colors indicate 0˚ and 90˚ plies, respectively. Red short lines are micro-cracks in 90˚ ply, and black short lines indicate interfacial delamination.)

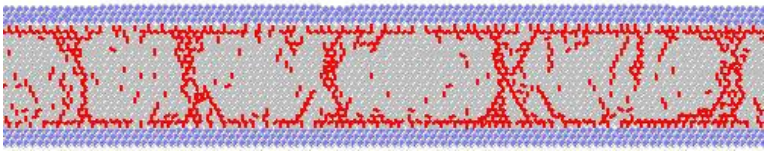

(a) without interfacial delamination

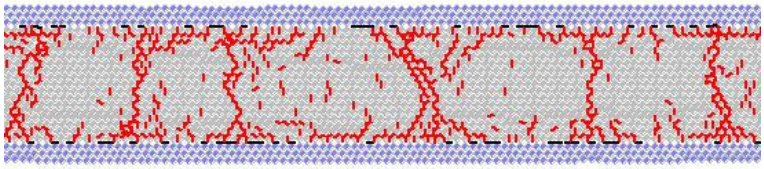

(b) with interfacial delamination

Fig.11 Magnified views of modeling at σ_c=294.3MPa

Fig.12 Typical transverse cracking saturation patterns in $[0^\circ_1/90^\circ_3]_s$ laminate [47]

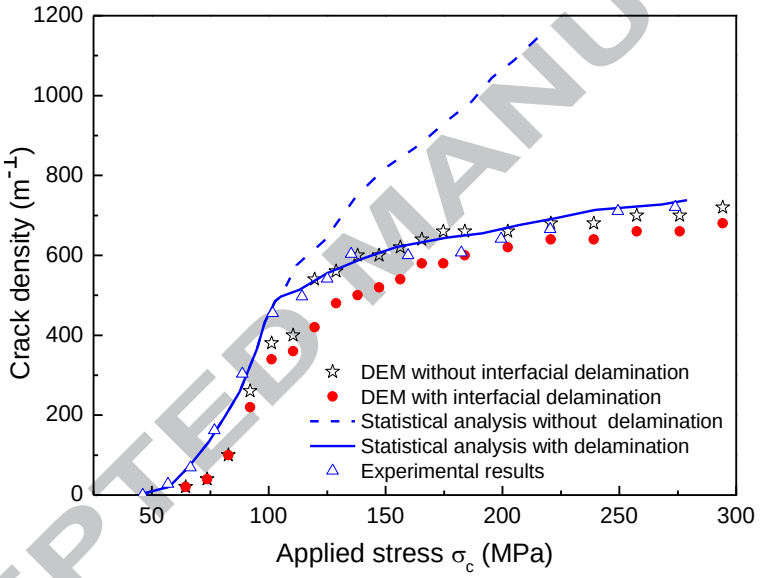

Fig.13 Transverse cracking density versus average applied stress in $[0^\circ_1/90^\circ_3]_s$ laminate

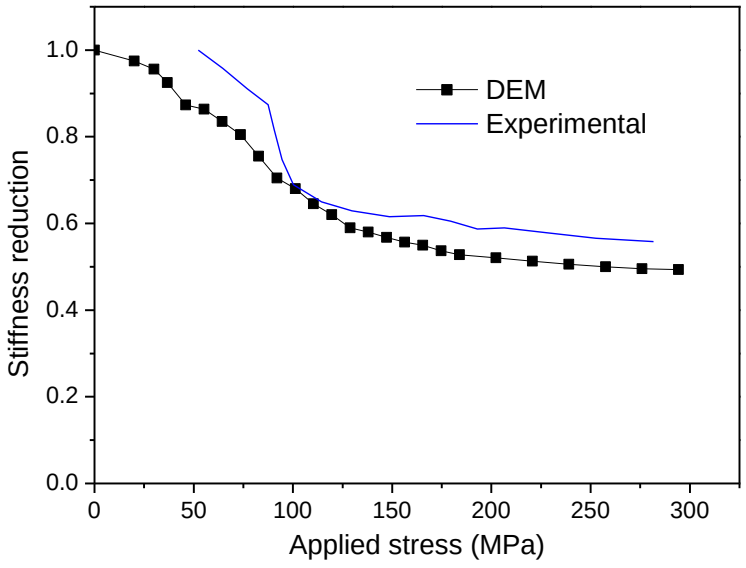

Fig.14 Stiffness reduction in $[0^\circ_1/90^\circ_3]_s$ laminate

The remaining stiffness of the specimen was also calculated from the corresponding loading stress and strain, and compared to the experimental results in [47] which are nominized in Fig.14. Comparable stiffness reduction rate from both the DEM modeling and experimental investigation can be observed. The reduced stiffness from the DEM model is always lower than the one from the test. This under estimated stiffness may be due to the fact that the experimental data were measured after the specimens were unloaded [47] during which some micro-cracks may be closed leading to a relative larger remaining stiffness, while the stiffness in DEM modeling was calculated directly by the stress and strain values at the exact loading points without the unloading and reloading process.

Simulations of the damage in $[90^\circ_n/0^\circ_1]_s$ cross-ply fiber reinforced composite laminates were also carried out using the similar DEM model. The material properties used in the simulations are as follows [27]:

For the 90º ply: E=9.6 GPa; υ=0.31
For the 0º ply: E_L=39.7 GPa; E_T=9.6 GPa; υ_{LT}=0.31; G_{LT}=4.5 GPa

The ply thickness is 90 μm. The average tensile strength of the 90˚ plies were assumed the same as the matrix yielding stress, σ_t =73 MPa, and the interface fracture energies G_{I} and G_{II} were 200 J/mm^2 and 400 J/m^2, respectively. Tensile strength of the 90˚ plies was assigned with a variation of 10% following the normal distribution law to account for the random failure taking place within the plies. Interface fracture energy was chosen with also a variation of 10%. As illustrated in Fig.15, the transverse cracks are almost uniformly distributed within all 90˚ plies. Unlike the $[0^\circ_1/90^\circ_n]_s$ laminates, the outside surfaces of the 90˚ plies in the $[90^\circ_n/0^\circ_1]_s$ laminates are more undulated and the detachment between the 0˚ and 90˚ plies at the delaminated position become more pronounced. This becomes even more obvious for the laminates with more 90˚ plies. This is due to the unsymmetrical stress distribution within the 90˚ plies since their outside surfaces are free of restraint. The thicker the 90˚ plies are, the larger the deformation caused by the unsymmetrical stresses will be. The extension of transverse cracks to the free surfaces at various positions of the 0˚ ply makes the stresses generated in the 90˚ plies also unsymmetrical and variable along the interfaces, causing the 0˚ ply exhibiting a bending type of deformation. The DEM simulations of damage were compared with the experimental investigations, as shown in Fig.16 [27], confirming that the detachment of the delaminated 90˚ plies and the deflection of the whole specimen were accurately captured by the DEM model. It was also found that the average length of the delamination zones increased with the thickness increase of the 90˚ plies.

In Fig.17, quantitative study of damage evolution was carried out by calculating crack density at various strains, and compared with the experimental results [27] and

the FEM solutions [27]. In the FEM models, special interfacial elements were required to be introduced into the 90˚ plies in order to initiate transverse cracks at the pre-defined positions. From the comparisons, good agreement was found in the development of crack density in all of the three laminates.

Furthermore, the curved propagation path of transverse cracking and the delamination, formed by both matrix cracking and interfacial failure, show a more comparable prediction than the FEM solution when compared with the experiments. Fig. 18 shows stiffness reduction obtained from the DEM simulation for the three laminates when they are subject to different levels of strains. All three laminates experienced sharp stiffness degradation after the loading is first applied. When the strain reaches a certain level, i.e., 1.0% in Fig.18, the rate of stiffness reduction becomes much smaller. Comparing Fig.18 with Fig.17, it can be observed that after the loading strain of 1.0% the remaining stiffness is almost constant, while the crack density is still increasing, especially in the $[90^\circ_1/0^\circ_1]_s$ and $[90^\circ_2/0^\circ_1]_s$ laminates. And it seems that the more 90˚ ply the laminate has, the slower the increase rate of crack density becomes. The reason for this is probably that large delamination length was formed in the laminates with thicker 90˚ plies, resulting in fewer transverse cracks within the space between any two existing transverse cracks, as indicated in Fig.15.

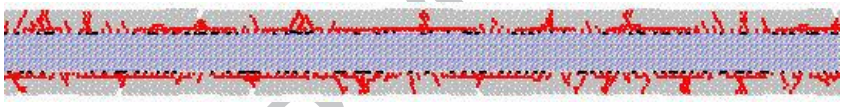

(a) $[90^\circ_1/0^\circ_1]_s$ laminate

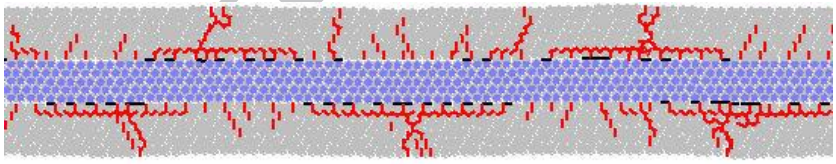

(b) $[90^\circ_2/0^\circ_1]_s$ laminate

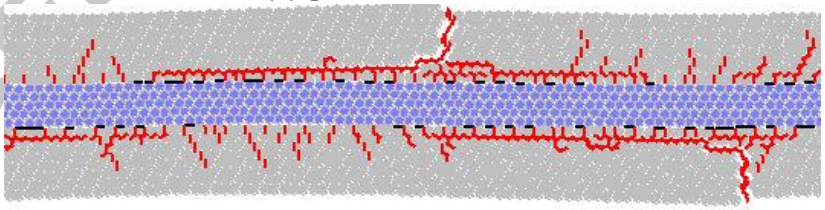

(c) $[90^\circ_3/0^\circ_1]_s$ laminate

Fig.15 Transverse cracking and delamination in $[90^\circ_n/0^\circ_1]_s$ cross-ply laminates at a loading strain of 2%. (Pictures were partially screen-printed with a length of 3mm)

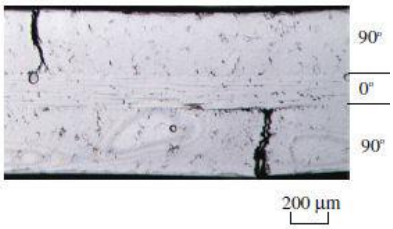

(a) $[90^\circ_2/0^\circ_1]_s$ laminate at 1.9% loading strain

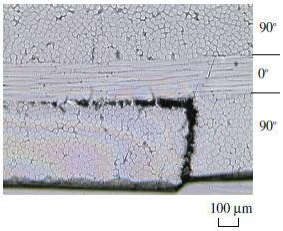

(b) $[90^\circ_3/0^\circ_1]_s$ laminate at 1.8% loading strain

Fig.16 Damage of $[90^\circ_n/0^\circ_1]_s$ cross-ply laminates observed in experiments [27]

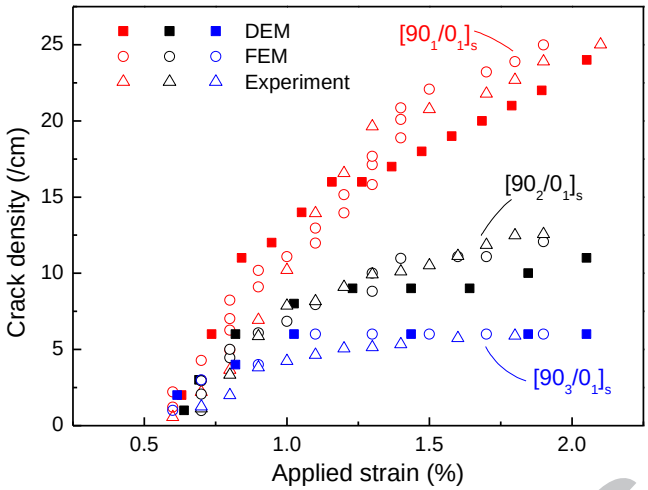

Fig.17 Transverse cracking density as a function of applied strain in $[90^\circ_n/0^\circ_1]_s$ cross-ply laminates

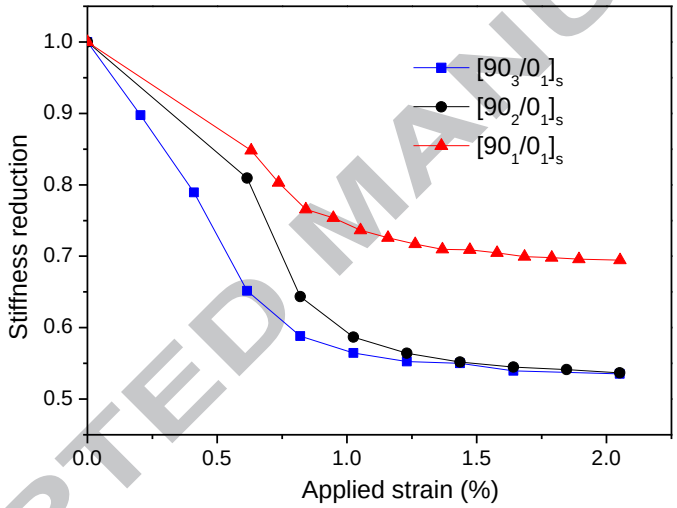

Fig.18 Stiffness reduction in $[90^\circ_n/0^\circ_1]_s$ laminate

6. Concluding remarks

The Discrete Element Method (DEM) has been employed to simulate dynamic initiation and propagation of transverse cracking as well as interfacial delamination in cross-ply laminates under uniaxial loading. The 90º and 0º plies were respectively treated as isotropic and orthotropic materials whose elastic properties were accounted by adopting the parallel bond model at the contacts of the discrete particles. The interface between the 90º and 0º plies was represented by a contact softening model. The developed DEM model was validated by comparing the stresses distribution in a representative element of cross-ply laminate with the results obtained from the analytical methods. As an application of the developed DEM model, the transverse cracking and interfacial delamination in both $[0^\circ_1/90^\circ_n]_s$ and $[90^\circ_n/0^\circ_1]_s$ cross-ply laminates under transverse loading were analyzed by comparing the calculated crack density with the experimental data and other numerical predications.

The comparisons shown that the DEM model is capable of not only modeling the

damage in laminates at microscopic particle level, but also capturing both the transverse cracking and delamination phenomenon, and predicting crack density as well as stiffness reduction quantitatively at macroscopic level.

The authors believe that further development of the model will enable more complicated damage in cross-ply laminates to be simulated by DEM, where more microstructure aspects, i.e., fiber volume, fiber diameter and fiber/matrix interface, and thus fiber breakage and fiber/matrix debonding can all be taken into account.

Acknowledgements

DM Yang would like to acknowledge the ORSAS scholarship and the University of Leeds studentship for the financial support to this research. YQ Tan would like to thank the NSFC of China for the financial support of this collaboration research under the Grant of No. 50875224.

References

[1] Hull D, Clyne TW. An introduction to composite materials. Cambridge University Press. 1996.

[2] Berthelot JM, Le Corre JF. A model for transverse cracking and delamination in cross-ply laminates. Composites Science and Technology. 2000;60(7):1055-1066.

[3] Dawe DJ, Lam SSE, Azizian ZG. Nonlinear finite strip analysis of rectangular laminates under end shortening, using classsical plate-theory. International Journal for Numerical Methods in Engineering. 1992;35(5):1087-1110.

[4] Bose P, Reddy JN. Analysis of composite plates using various plate theories Part 1. Formulation and analytical solutions. Structural Engineering and Mechanics. 1998;6(6):583-612.

[5] Reddy JN. A generalization of two-dimensional theories of laminated composite plates. Communications in Applied Numerical Methods. 1987;3(3):173-180.

[6] McCartney L, Pierse C. Stress transfer mechanics for multiple ply laminates for axial loading and bending. In: Proceeding of the 11th International Conference on Composite Materials, Gold Cost, Australia. 1997;July 14-18:662-671.

[7] McCartney LN. New Theoretical Model of Stress Transfer Between Fibre and Matrix in a Uniaxially Fibre-Reinforced Composite. Proceedings of the Royal Society of London Series A, Mathematical and Physical Sciences. 1989;425(1868):215-244.

[8] Carreira RP, Caron JF, Diaz AD. Model of multilayered materials for interface stresses estimation and validation by finite element calculations. Mechanics of Materials. 2002;34(4):217-230.

[9] Ye JQ, Sheng HY. Free-edge effect in cross-ply laminated hollow cylinders subjected to axisymmetric transverse loads. International Journal of Mechanical Sciences. 2003;45(8):1309-1326.

[10] Ye JQ, Sheng HY, Qin QH. A state space finite element for laminated composites with free edges and subjected to transverse and in-plane loads. Computers & Structures. 2004;82(15-16):1131-1141.

[11] Leblond P, ElMahi A, Berthelot JM. 2D and 3D numerical models of transverse cracking in cross-ply laminates. Composites Science and Technology. 1996;56(7):793-796.

[12] Nairn JA. The Strain Energy Release Rate of Composite Microcracking: A Variational Approach. Journal of Composite Materials. 1989;23(11):1106-1129.

[13] Wang J, Karihaloo BL. Matrix crack-induced delamination in composite laminates under transverse loading. Composite Structures. 1997;38(1-4):661-666.

[14] Chen J, Crisfield M, Kinloch AJ, Busso EP, Matthews FL, Qiu Y. Predicting Progressive Delamination of Composite Material Specimens via Interface Elements. Mechanics of Composite Materials and Structures. 1999;6(4):301 - 317.

[15] Bruno D, Greco F, Lonetti P. A coupled interface-multilayer approach for mixed mode delamination and contact analysis in laminated composites. International Journal of Solids and Structures. 2003;40(26):7245-7268.

[16] Wagner W, Gruttmann F, Sprenger W. A finite element formulation for the simulation of propagating delaminations in layered composite structures. International Journal for Numerical Methods in Engineering. 2001;51(11):1337-1359.

[17] Nishikawa M, Okabe T, Takeda N. Numerical simulation of interlaminar damage propagation in CFRP cross-ply laminates under transverse loading. International Journal of Solids and Structures. 2007;44(10):3101-3113.

[18] Hu N, Zemba Y, Fukunaga H, Wang HH, Elmarakbi AM. Stable numerical simulations of propagations of complex damages in composite structures under transverse loads. Composites Science and Technology. 2007;67(3-4):752-765.

[19] Meo M, Thieulot E. Delamination modelling in a double cantilever beam. Composite Structures. 2005;71(3-4):429-434.

[20] Borg R, Nilsson L, Simonsson K. Simulation of delamination in fiber composites with a discrete cohesive failure model. Composites Science and Technology. 2001;61(5):667-677.

[21] Pantano A, Averill RC. A mesh-independent interface technology for simulation of mixed-mode delamination growth. International Journal of Solids and Structures. 2004;41(14):3809-3831.

[22] Xie D, Waas AM. Discrete cohesive zone model for mixed-mode fracture using finite element analysis. Engineering Fracture Mechanics. 2006;73(13):1783-1796.

[23] Maimí P, Camanho PP, Mayugo JA, Dávila CG. A continuum damage model for composite laminates: Part I - Constitutive model. Mechanics of Materials. 2007;39(10):897-908.

[24] Camanho PP, Maimí P, Dávila CG. Prediction of size effects in notched laminates using continuum damage mechanics. Composites Science and Technology. 2007;67(13):2715-2727.

[25] Blázquez A, Mantic V, París F, McCartney LN. Stress state characterization of delamination cracks in [0/90] symmetric laminates by BEM. International Journal of Solids and Structures. 2008;45(6):1632-1662.

[26] Berthelot JM, Le Corre JF. Statistical analysis of the progression of transverse cracking and delamination in cross-ply laminates. Composites Science and Technology. 2000;60(14):2659-2669.

[27] Okabe T, Nishikawa M, Takeda N. Numerical modeling of progressive damage in fiber reinforced plastic cross-ply laminates. Composites Science and Technology. 2008;68(10-11):2282-2289.

[28] Yang D, Sheng Y, Ye J, Tan Y. Discrete element modeling of the microbond test of fiber reinforced composite. Computational Materials Science. 2010;49(2):253-259.

[29] Sheng Y, Yang D, Tan Y, Ye J. Microstructure effects on transverse cracking in composite laminae by DEM. Composites Science and Technology.70(14):2093-2101.

[30] Cundall PA, Strack ODL. A discrete mumerical model for granular assemblies. *Géotechniqu*. 1979;29(1):47-65.

[31] Hunt SP, Meyers AG, Louchnikov V. Modelling the Kaiser effect and deformation rate analysis in sandstone using the discrete element method. Computers and Geotechnics. 2006;30:611-621.

[32] Sheng Y, Lawrence CJ, Briscoe B, Thornton C. Numerical studies of uniaxial powder compaction process by 3D DEM. Engineering Computations: International Journal for Computer-Aided Engineering. 2004;21(2-3):304-317.

[33] Frédéric SH, Donzé V, Daudeville L. Discrete element modeling of concrete submitted to dynamic loading at high strain rates. Computers & Structures. 2004;82:2509-2524.

[34] Tan Y, Yang D, Sheng Y. Study of polycrystalline Al2O3 machining cracks using discrete element method. International Journal of Machine Tools and Manufacture. 2008;48(9):975-982.

[35] Itasca Consulting Group Inc. PFC2D (particle flow code in 2-dimensions), Version 3.10, User Mannual. Minneapolis, Minnesota. 2004.

[36] Potyondy DO, Cundall PA. A bonded-particle model for rock. International Journal of Rock Mechanics and Mining Sciences. 2004;41(8):1329-1364.

[37] Wittel FK, Kun F, Kröplin B-H, Herrmann HJ. A study of transverse ply cracking using a discrete element method. Computational Materials Science. 2003;28(3-4):608-619.

[38] Sawamoto Y, Tsubota H, Kasai Y, Koshika N, Morikawa H. Analytical studies on local damage to reinforced concrete structures under impact loading by discrete element method. Nuclear Engineering and Design. 1998;179(2):157-177.

[39] Kim H, Wagoner MP, Buttlar WG. Simulation of fracture behavior in asphalt concrete using a heterogeneous cohesive zone discrete element model. Journal of Materials in Civil Engineering. 2008;20(8):552-563.

[40] Tavarez FA, Plesha ME. Discrete element method for modelling solid and particulate materials. International Journal for Numerical Methods in Engineering. 2007;70(4):379-404.

[41] Liu K, Liu W. Application of discrete element method for continuum dynamic problems. Archive of Applied Mechanics. 2006;76(3-4):229-243.

[42] Itasca Consulting Group Inc. PFC2D (particle flow code in 2-dimensions), Version 3.10. Minneapolis, Minnesota. 2004.

[43] Borg R, Nilsson L, Simonsson K. Modeling of delamination using a discretized cohesive zone and damage formulation. Composites Science and Technology. 2002;62(10-11):1299-1314.

[44] Li S, Thouless MD, Waas AM, Schroeder JA, Zavattieri PD. Use of a cohesive-zone model to analyze the fracture of a fiber-reinforced polymer-matrix composite. Composites Science and Technology. 2005;65(3-4):537-549.

[45] Yang D, Ye J, Tan Y, Sheng Y. Modeling progressive delamination of laminated composites by discrete element method. Computational Materials Science. 2011;50(3):858-864.

[46] Zhang D, Ye J, Sheng HY. Free-edge and ply cracking effect in cross-ply laminated composites under uniform extension and thermal loading. Composite Structures. 2006;76(4):314-325.

[47] Highsmith AL, Reifsnider KL. Stiffness reduction mechanisms in composite laminates. ASTM STP 775. 1982:103-117.

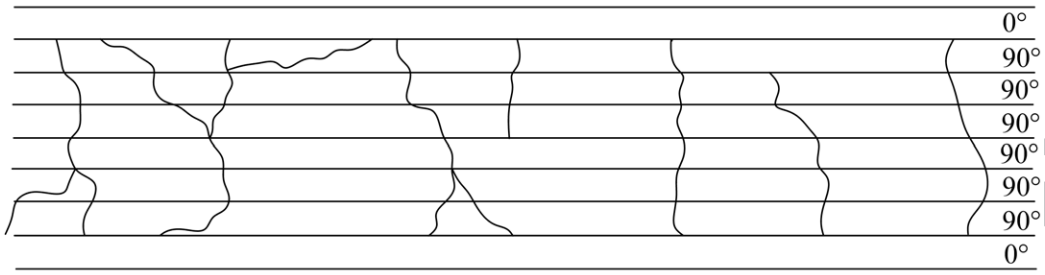

>We model cross-ply laminates by particle based discrete elements. > We examine dynamic process of transverse cracking and interface delamination. > We examine the interaction between transverse cracking and delamination. > Stiffness reduction is studied against crack density with and without delamination.